PAPER

Check for updates

The effect of Si/Al ratio and drug loading level on the molecular behaviour and controlled release of 5-fluorouracil from zeolite H-Beta†

G. A. Dunkley, [ID] [a] S. L. McHugh,[a] A. J. Porter,[a] A. J. Wise,[b] M. Appel, [ID] [c] P. A. Cox[b] and A. J. O'Malley [ID] *[a]

The controlled release of anticancer drug 5-fluorouracil (5FU) from zeolite H-Beta has been studied with varying zeolite composition (Si/Al = 19 and 180), and correlated with its molecular behaviour, studied by quasielastic neutron scattering (QENS) and classical molecular dynamics simulations. The study aimed to understand the effect of increasing the Brønsted acid adsorption site concentration on the release properties of these potential drug delivery materials. A factor of ∼1.5 more 5FU was released from the sample with Si/Al = 180 over the release period, consistent with TGA analysis showing a factor of ∼1.5 more drug was encapsulated in this sample, which may initially seem counterintuitive given that it contains far fewer adsorption sites. Notably, the scale parameter of release from the H-Beta sample with Si/Al = 19 was slightly faster, despite the lower total loading and therefore final amount released from this sample. This slightly faster relative release rate was initially attributed to a lower level of steric 'crowding' between 5FU molecules in the H-Beta-19 pore system and thus hindrance to molecular mobility compared to H-Beta-180, consistent with the lower observed molecular loading level. QENS studies probing 5FU molecular motions observed the 5FU to be undergoing localised diffusion in the zeolite Beta intersections in both samples, with a higher proportion of mobile molecules performing this motion in H-Beta-19. This suggested the increased total drug loading in H-Beta-180, and resulting steric hindrance in the pore system, is the significant factor in adsorbed drug behaviour, and potentially the relative release rate from these zeolites. Molecular dynamics simulations probed the effect of increasing the drug loading level in the Beta framework and supported that increasing molecular loading significantly hindered total drug mobility due to favourable molecule–molecule interactions in the pore system. The study illustrates the complex relationship between zeolite composition, resulting drug loading level, molecular behaviour, and subsequent release profiles in the design of microporous controlled release systems for anticancer drug delivery.

1. Introduction

Drug delivery systems (DDS) have been shown to reduce side effects by decreasing dosing frequency, protecting a drug until it reaches its target area, and even potentiating the effect of the drug.[1–5] Crucially, the encapsulation of a drug within a DDS may lead to less drug waste, improved patient compliance and a more personalised approach to treatment.[6] 5-Fluorouracil

(5FU) is an antimetabolite drug used to treat conditions such as colorectal cancer, stomach and breast cancer and as a topical treatment for some skin cancers.[7] However, 5FU induces significant toxic side effects, intravenous administration causes significant issues, and patient preference would generally be for administration orally or through a skin patch.[6] Thus, 5FU would be an attractive candidate for encapsulation into a controlled release dosage form.

Various materials have been considered for DDSs, including nanoparticles,[8] silicon disks,[9] metal organic frameworks (MOFs),[10] and zeolitic imidazolate frameworks (ZIFs).[11] Release systems for 5FU have also been devised from double-layered nanosheets,[12] and conjugates based on quantum dots.[13] However, zeolites are also emerging as a promising new material for drug release due to the variety of framework topologies and pore sizes suitable for the accommodation of different drug

[a] Department of Chemistry and Institute of Sustainability and Climate Change, University of Bath, Claverton Down, Bath BA2 7AY, UK. E-mail: a.o'malley@bath.ac.uk

[b] School of Medicine, Pharmacy and Biomedical Sciences, University of Portsmouth, White Swan Road, Portsmouth PO1 2DT, UK

[c] Institut Laue-Langevin (ILL) 71 Av. Des Martyrs, 38000 Grenoble, France

† Electronic supplementary information (ESI) available. See DOI: https://doi.org/10.1039/d5tb00256g

molecules and their 'green'/non-toxic methods of synthesis. Zeolites show promising results especially in the area of theranostics[14] and readers are directed towards a review by Bacakova et al. detailing the use of zeolites in biotechnology and medicine.[15]

Zeolites are generally considered biocompatible, for example the Food and Drug Administration (FDA) has approved silica for use in the body, and it is a commonly used food additive (E551).[16] Moreover, zeolites are already used in medical devices, such as QuikClot® – a wound dressing that helps promote clot formation. It is important to note, however, that some zeolites are cytotoxic or carcinogenic, particularly if they form fibrous needle-like crystals, such as erionite, offretite and scolecite; thus, it is paramount to select zeolite frameworks without these properties and perform cytotoxicity investigations for some zeolite frameworks.

Zeolites are microporous, crystalline aluminosilicates, which contain periodic pores and channels with tuneable molecular dimensions. They are composed of tetrahedral building blocks of either a silicon or an aluminium atom surrounded by four oxygen atoms. The negative charge invoked on the neighbouring oxygen due to the inclusion of aluminium instead of silicon is balanced by the introduction of cations, such as positive metal ions (positioned as extraframework ions) or protons attached to the oxygen and acting as Brønsted acid sites.[17] The Si/Al ratio affects the concentration of cations present in the material, which drug molecules that enter the channel structure may strongly adsorb to. Indeed, recent studies of the release of drugs such as atenolol have shown markedly different release profiles with varying composition, including zero order release at certain FAU zeolite compositions.[18] Thus, varying the Si/Al ratio in zeolites is of significant interest for the design and optimisation of DDSs, as it can alter the uptake of drugs, their interactions within the pore, and ultimately their controlled release rate.

Zeolite Beta forms intergrown compact non-fibrous crystals, which are not considered to be cytotoxic, as documented by SEM imaging in the literature.[19] It has a 3D network of intersecting channels of approximately $\sim$6.5 Å diameter which are ideal for the accommodation of 5FU, and is available commercially in a range of Si/Al ratios. Whilst there have been studies probing the effect of pore size and shape on the release of 5FU from zeolites,[19,20] very few studies have taken place concerning the effect of Si/Al ratio. Datt et al.[21] investigated the loading and release of 5FU from larger-pore HY zeolites with varying Si/Al ratios and found that, while composition does have an effect on 5FU loading and the final amount released, no "controlled" release was observed, with the zeolites completely releasing the drug in $\sim$10 minutes. It was observed, however, that the zeolite with the lowest Si/Al ratio and thus the highest concentration of counterions (Si/Al = 2.5) showed almost no drug release at all. More recently, Fischer computationally investigated the adsorption of 5FU in faujasite, specifically probing systems with varying numbers of Brønsted acid sites per 12-membered ring, and concluded that strong hydrogen bonding does indeed occur between carbonyl functional groups on 5FU and the acid sites, implying that acid site presence would reduce encapsulated drug

motion and thus potentially the rate of drug release.[22] Al-Thawabeia et al.,[23] however, reported an experimental increase in 5FU release rate from ZSM-5 when using the proton form of the zeolite over the sodium form. To our knowledge, these are the only studies probing the effect of zeolite composition and Si/Al ratio on 5FU interactions and release from zeolites, and highlight how the relationship between zeolite composition, interactions with 5FU, and resulting release is far from simple.

For studying the interactions and subsequent dynamics of molecules adsorbed in zeolites on the nanoscale, neutron scattering techniques offer significant insight due to their unique sensitivity to hydrogenous molecules, their highly penetrative nature, and the minimal interaction of neutrons with the inorganic zeolite framework.[24] Therefore, only the dynamics of the adsorbed molecule, in this case the 5FU, would be detected. Quasielastic neutron scattering (QENS) has shown to be particularly revealing in terms of understanding the diffusion mechanisms[25,26] and rotational behaviour[27,28] of molecules in zeolites, typically in the context of microporous catalysis.[24] The technique is based on neutrons with scattered energies on the order of μeV from their interactions with molecules undergoing translational or rotational motions. This allows for drug diffusion rates and mechanisms to be extrapolated, as demonstrated for paracetamol and ibuprofen in delivery systems based on supramolecular gel fibre hosts by Edkins et al.[29] In the case of zeolites, where drug mobility through the framework can be pivotal to the release rate, the combination of QENS and classical molecular dynamics (MD) simulations has shown to be very powerful in gaining a detailed understanding of local and nanoscale molecular behaviour in microporous materials, as these techniques sample the same time and length scales.[30,31] While this combination can offer unique insight into the qualitative and quantitative characteristics of molecular behaviour in porous materials (particularly for bulky cyclic/functionalised molecules similar to pharmaceutically relevant species[32–36]) it is to our knowledge, yet to be applied to a system relevant to the use of porous inorganics for controlled drug delivery applications.

Herein, the effect of Si/Al ratio on the molecular behaviour of 5FU in zeolite H-Beta as studied by QENS and MD simulations is reported, and the correlation with its controlled release from the zeolite in a pH neutral environment using H-Beta samples with Si/Al = 19 and 180 (3 and 0.33 Brønsted acidic adsorption sites per unit cell respectively). It is shown that the change in the number of Brønsted acid sites has significant effects on the uptake of 5FU, subsequent influences on the dynamical behaviour of 5FU in the pores, and the resulting drug release rates and profiles.

2. Methods

2.1 Materials and drug encapsulation

5FU form I crystal (product code 11906531, China), zeolite NH₃-Beta with a Si/Al = 19 (product code 15402507, surface area 710 m² g⁻¹, Heysham, UK) and H-Beta with a Si/Al = 180

This journal is © The Royal Society of Chemistry 2025

J. Mater. Chem. B, 2025, 13, 10314–10330 | 10315

(product code 15432507, surface area 620 m^2 g^{-1}, Haverhill, USA) were purchased from Fisher Scientific. The ammonium form of Beta (Si/Al = 19) was converted to the proton form through calcination at 823 K for 5 hours after being heated to that temperature at a rate of 1 K min^{-1}. The Si/Al = 19 and 180 zeolite Beta samples are referred to herein as H-Beta-19 and H-Beta-180. Pre-treatment of the zeolites before 5FU encapsulation included drying them at 393 K under vacuum for 12 hours to remove any weakly bound water. Encapsulation of the 5FU into the zeolite drug delivery system (DDS) was achieved *via* the following mixing procedure: 2.4 g of 5FU was dissolved in 300 mL of ethanol and 4 g of H-Beta-180 was added straight from its sealed drying vessel, with the same carried out for H-Beta-19. The samples were stirred at 300 rpm for 24 hours, filtered while washing with ethanol (to remove any residual non-adsorbed 5FU) and dried for 30 minutes at 333 K to ensure all ethanol was evaporated. The resulting DDS samples are referred to herein as H-Beta19-5FU and H-Beta180-5FU for the Si/Al = 19 and 180 samples respectively.

2.2 Characterisation

The non-loaded zeolites and the loaded DDSs were characterised using X-ray diffraction (XRD) and thermogravimetric analysis (TGA), which will now be discussed. The procedures for TGA and XRD and analysis are outlined in Section S1.1 and S1.2 respectively (ESI†). XRD patterns of the non-loaded zeolite, the drug-loaded DDS and the drug alone are shown in Fig. S3 and S4 (ESI†). They indicate that no crystalline 5FU is present in the DDS, and that the bulk crystallinity/integrity of the zeolite frameworks were not affected by the encapsulation of 5FU. Some changes in relative Bragg peak heights and broadenings (discussed in Section S1.2, ESI†) were observed in the zeolite XRD patterns, a common occurrence upon adsorption of a species in the zeolite pore system.[19,23,37,38] It is possible that a small portion of the 5FU is adsorbed onto the surface of the zeolite; however, the absence of the bulk 5FU crystalline structure in the DDS, and the TGA results discussed later suggest that most of the drug molecules are likely confined within the pores. We note that the XRD patterns were typical for Beta type zeolites, which along with the very large internal surface areas (620 and 710 m^2 g^{-1}) confirm the microporous structure of the zeolite samples. XRD traces were also taken for the zeolites post-drug release, and again showed that the zeolite was unaffected (Fig. S5, ESI†).

2.3 Drug release studies

To investigate the release profile of 5FU from both zeolite systems, drug release studies were performed. A UV-vis calibration curve was determined for 5FU in phosphate buffered saline (PBS), ranging from 0.001 mg mL^{-1} to 1 mg mL^{-1}. Drug release studies were performed over 120 minutes in PBS, pH 7.4 which mimics the conditions of the intestines and interstitial fluids, provides a standardised reference, and is a more accurate comparison with the QENS experiments and MD simulations. The PBS was prepared in 1 L batches, using Oxoid PBS tablets (Procured from Thermo Fischer, Scheepsbouwersweg, The Netherlands) (1 tablet per 100 mL of distilled water). Pellets

were prepared for each DDS; $\sim$100 mg of DDS was present in each pellet. Each pellet was pressed using 5 tonnes of pressure for 30 seconds using a Specac® Atlas 15T manual hydraulic press. The pellet was added to a vessel of 4 cm diameter with uniform openings of approx. 500 μm as in the basket form of a standard dissolution apparatus. This vessel was suspended in 200 mL of PBS, which was stirred at 300 rpm. 1.5 mL aliquots were removed at defined time points and the absorbance of the aliquot was read using a UV-vis analyser at λ = 296 nm (Perkin-nElmer, model- Lambda 650s, serial number: 650L1411071). 1.5 mL of fresh PBS was added immediately after each aliquot was taken to maintain a volume of 200 mL. To correct for the dilution effect of replacing the aliquots, the following equation[39] was used to calculate the amount of 5FU released:

$$C_{t\text{corr}} = C_t + \frac{v}{V} \sum_0^{t-1} C_t \qquad (2.1)$$

Where $C_{t\text{corr}}$ is the corrected concentration at time t. C_t is the concentration at time t, v is the volume of the aliquot taken and V is the total volume of the PBS. Experiments were performed in triplicate and the results were averaged.

2.4 Quasielastic neutron scattering experiments

Empty and loaded zeolite samples were vacuum dried at 473 K overnight (approx. 13 hours) in a quartz tube to ensure the maximum amount of water possible was removed (without degrading the confined drug molecules). The sealed quartz tube was transferred to a glove box where approximately 2 g of each DDS and each non-loaded zeolite was inserted in a 6 cm × 12 cm aluminium envelope which was evenly rolled to 1 mm thickness, and then rolled into a cylinder and positioned in aluminium cylindrical cans. The ends of the filled envelopes did not overlap within the cylinder to avoid multiple scattering from the sample. Thin walled, lead wire sealed aluminium cans of annular geometry were used for the QENS experiment, the Al foil envelopes were inserted into the cans which were then sealed and heated to ensure an airtight lead seal. The back-scattering and time of flight (BATS) option on the IN16B spectrometer at the ILL (Grenoble)[26] was used with Si (111) analyser crystals, with the chosen chopper settings using a 14° slit in the pulse choppers at 315.4 Hz corresponding to an energy resolution of $\sim$5 μeV FWHM, sampling $\sim$300 ps time-scales. The detector covered measurements over a Q range of 0.2 to 1.9 Å^{-1}. The filled sample cans were inserted into a cryofurnace mounted on the spectrometer for temperature control. The neutron scattering recording time was approximately 2 hours per spectrum per temperature. Four samples were measured, H-Beta (Si/Al = 19) without drug (H-Beta-19), H-Beta (Si/Al = 19) with 5FU encapsulated (H-Beta19-5FU), H-Beta (Si/Al = 180) without drug (H-Beta-180) and H-Beta (Si/Al = 180) encapsulated with 5FU (H-Beta180-5FU). Each sample was cooled to a base temperature of 2 K and a resolution measurement was taken. The samples were then heated and measurements were taken at 300 K. All data were reduced using standard routines, correcting for empty can background signal

and self-absorption. Subsequently, measurements taken of the non-dosed zeolites had their (comparatively small) resulting signal subtracted from that of the drug containing samples. (H-Beta19-5FU and H-Beta180-5FU) signal, therefore, only the signal from the drug molecule was investigated. The data were reduced using the Mantid 6.2.0[40] software and analysed using the DAVE[41] software.

2.5 Molecular dynamics simulations

Zeolite Beta consists of a framework of intersecting channels formed by 12 membered rings of diameter ~6.7 Å.[42,43] The siliceous orthorhombic unit cell of Beta (BEA) consists of 192 atoms.[44,45] The unit cell was then extended by $4 \times 4 \times 2$ in the a, b and c directions respectively, to create a supercell of approx. 6200 atoms, as seen in Fig. 1. Periodic boundary conditions were employed.

A flexible zeolite potential model was used as previous work has shown it to be necessary to accurately model dynamics of adsorbed larger molecules.[46] Non-bonded interactions were described using the potentials of Schröder et al. and Sanders et al.[47,48] The Si–O and O–O interactions were described by Buckingham potentials, and are listed in Table S1 (ESI†). Full ionic charges were applied. The three body potential for the O–Si–O angles used was from the work of Ramsahye and Bell.[49] All potentials were derived from ab initio methods and fitting to experimental data performed on zeolites and alpha quartz. The empty frameworks were equilibrated at 300 K for 100 ps in the canonical (NVT) ensemble, using a Berendsen thermostat and a time step of 0.5 fs.

Once the frameworks were equilibrated, 5FU drug molecules were added to both framework systems in loadings of 4, 6, 10 and 15 wt% per supercell, corresponding to ~1, ~1.5, ~3 and ~5 5FU molecules per unit cell. Full information regarding the loadings for each system may be found in Table S2 (ESI†). The equilibrated Beta supercell loaded with 4 wt% 5FU is shown in Fig. 1. Note that these are lower loadings than were encapsulated in the experimental samples for the QENS experiments, where in order to maximise the scattered neutron flux in the experiments and achieve the best statistics for our experiment, higher loadings were achieved as detailed in Section 3.1. However, in terms of comparing the effect of loading on dynamics, reliable comparisons may be made over the modelled loading range of 4–15 wt% as discussed in later sections.

The 5FU molecules were described using potentials from the CVFF force field,[50] using charges from the work of Abdel-Mottaleb who used DFT and its time-dependent extension (TD-DFT) to model the optimised structures and molecular properties related to uracil derivatives including 5-fluorouracil.[51] The Lennard-Jones potential[52] in the σ and ε form are used to approximate the intermolecular potential energy between each pair of 5FU atoms. The Lorentz–Berthelot[53] mixing rules were used to combine the σ and ε values of the zeolite and the 5FU molecules, resulting in Lennard-Jones potentials for all interactions, listed in Table S3 (ESI†). The 5FU loaded zeolite systems were equilibrated for 1 ns using the procedure mentioned previously at 300 K.

The DLPOLY 4[54] code was used for all MD simulations, with a time step of 0.5 fs, a van der Waals cut-off of 12 Å, with the Coulombic interactions solved using the Ewald summation method.[55] After reaching equilibration as described above, production runs of 2 ns in length in the microcanonical (NVE) ensemble were performed. The positions of all atoms in the system were recorded every 0.5 ps. The self-diffusion coefficient of the 5FU molecules was not determined as the log(MSD)–log(t) relationship in relation to the Einstein relation was not linear over the modelled timescale, so translational diffusion was not taking place.

To determine the localised motions of the drug molecules within the zeolite framework, QENS observables, such as the intermediate scattering function (ISF) and the elastic incoherent structure factor (EISF) were reproduced using the following equations.

$$F_s(Q,t) = \frac{1}{N} \sum_{i=1}^{N} \left\langle \frac{\sin(Q|d_i(t+t_0) - d_i(t_0)|)}{Q|d_i(t+t_0) - d_i(t_0)|} \right\rangle \quad (2.2)$$

Where N is the total number of atoms and d_i is the atomic coordinates of one of the hydrogen atoms at time t. Reproducing these observables allowed for direct comparison with the QENS experiments.

To allow for better statistics, the multiple time origin method was used when calculating the ISF. 500 $\times$ 500 ps trajectories, each offset by 3 ps were created which covered the entire 2 ns production run. The ISFs generated from these were fit using the following exponential function:

$$F_s(Q,t) = B(Q) + \sum_{n=0}^{i} C_n e^{-\Gamma_n t} \quad (2.3)$$

where i is the number of exponentials and $B(Q) + \sum_{n=0}^{i} C_n = 1$.

This $B(Q)$ term is related to the EISF. The $B(Q)$ or 'baseline' of the exponential can be plotted as a function of Q to directly compare the motions observed between simulation and experiment.[56]

Further 200 ps production runs were performed with atomic positions recorded every 0.05 ps, from which the angular correlation functions (ACFs) were calculated using the eqn (2.4),

$$\text{ACF}_{g,i}(t) = \langle v_{t,i}(0) \cdot v_{t,i}(t) \rangle, \quad i = 1, 2, 3 \quad (2.4)$$
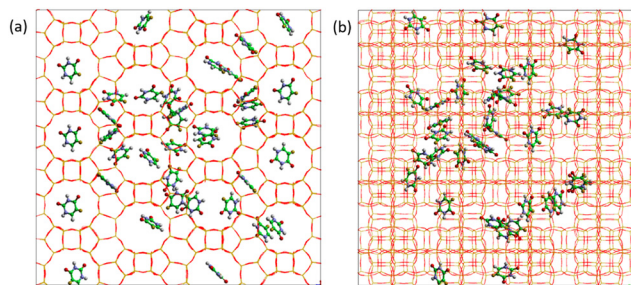

Fig. 1 Beta framework supercell loaded with 4 wt% 5FU, viewed down the (a) 100 and (b) 001 direction respectively.

where g is a triplet of non-colinear atoms and v_i are a series of orthonormal vectors derived from the triplet.[57]

This allowed determination of the rotational diffusion coefficient (D_r) of 5FU through fitting of an exponential function to the ACF decay, where the rate of decay with respect to time is proportional to the rate of rotation, as in eqn (2.5).[58]

$$ACF(\Delta t) = e^{-6D_r\Delta t} \qquad (2.5)$$

The adsorption energy (E_{ads}) for 5FU in siliceous Beta was calculated using minimum energy geometry optimisation calculations for an empty Beta unit cell, a Beta unit cell with 1 loaded 5FU molecule, and 5FU alone. The 5FU E_{ads} was calculated with the following equation:

$$E_{ads} = E_{5FU+zeolite} - \left(E_{5FU} + E_{zeolite}\right) \qquad (2.6)$$

3. Results and discussion

3.1 Thermogravimetric analysis

Thermogravimetric analysis (TGA) was used to determine the loading of each zeolite framework with 5FU. Two distinct events are seen in the TGA plot (Fig. 2), the first is the loss of physisorbed water at ~ 373 K, while the second event which is of far greater magnitude occurs at $\sim 533-623$ K, attributable to the decomposition of the 5FU molecules from within framework pores. The sublimation temperature range of the 5FU form I crystal, derived from pure 5FU TGA (Fig. S1, ESI†), is 515–610 K. Therefore, the prolonging of the second event to higher temperatures indicates that there is 5FU residing within the pores of the zeolite, rather than just being present on the surface of the zeolite particles, and is benefiting from degradation protection. While there is a possibility of 5FU molecules adhering to the crystallite surface, the washing step used to remove surface bound drug during the encapsulation process, our XRD analysis, (discussed in Section S1.2, ESI†) and the very

favourable adsorption energies calculated for 5FU confinement in the zeolite framework (>150 kJ mol^{-1})[19] leads us to conclude that the vast majority of drug would be confined in the micropores. The initiation of 5FU related weight loss at temperatures below the region observed for pure 5FU (highlighted in yellow) can be attributed to a small amount of 5FU adsorbed to the zeolite surface, which is less stabilised than crystalline drug species, or drug molecules confined within the zeolite pores. Adsorption energies for 5FU on zeolite surfaces have been reported in the range 58–79 kJ mol^{-1},[59] thus far lower than those associated with confinement. The derivative of each TGA dataset is present in the figure also as a visual aid to observe each event.

It can therefore be concluded that the H-Beta-180 sample encapsulated/adsorbed a larger amount of 5FU than H-Beta-19 by a factor of ~ 1.5 (37 wt% compared to 25 wt%). A potential reason for this may be the presence of far more acidic sites in the H-Beta-19 system to which 5FU molecules (and solvent) will hydrogen bond. These H-bonded molecules may cause steric hindrance to the passage of other 5FU molecules through the channels and reduce the available pore space (as seen previously for other cyclic H-bonding molecules such as cresols in the same zeolite structure[32]) hindering further adsorption of 5FU molecules. Therefore, the higher loading capacity of H-Beta-180 may be, perhaps counterintuitively, due to the lack of these adsorption sites and their respective hindrances to mobility and resulting uptake. TGA of the non-drug dosed zeolites, either exposed only to atmosphere, or deliberately saturated with water in a humid environment can be found in Fig. S2, and discussed in Section S1.1 (ESI†), and show that H-Beta-19 has a higher affinity for water both due to the quantities taken up under both conditions, and the profile of water desorption. The increased hydrophilicity of H-Beta-19 may explain the lower 5FU loading achieved, as hydrophobic non-polar interactions may be more encouraged in the almost fully siliceous H-Beta-180 structure.

The TG analyses also suggest that each DDS is stable, since the sample was stored for a minimum of 72 hours after encapsulation before TGA measurements were taken, and still showed that 5FU was encapsulated within the Beta zeolites, stable up to ~ 533 K. PXRD patterns taken for the empty and loaded zeolites (Section S1.2, ESI†) corroborated that each DDS is stable post-loading.

3.2 Controlled drug release studies

The release profiles of 5FU from zeolite H-Beta180-5FU and H-Beta19-5FU, are shown in Fig. 3, the data are the average of triplicate experiments, and the error bars are smaller than the data points. Upon calculating concentrations relative to those obtained from the TGA measurements, approximately 93% of the encapsulated drug was released after 120 minutes from H-Beta-180, and approximately 98% of the encapsulated drug was released after 120 minutes from H-Beta-19. Approximately 1.5 times more drug is released from the H-Beta-180 system than the H-Beta-19 system overall, in accordance with the observation that a factor of 1.5 more was encapsulated.
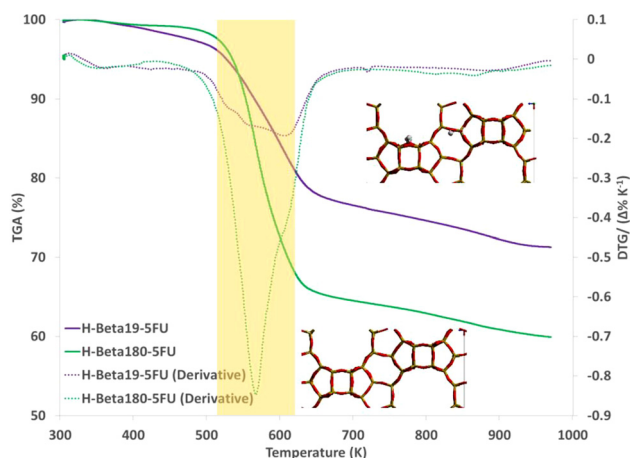

Fig. 2 TGA of H-Beta19-5FU DDS (purple) and H-Beta180-5FU DDS (green), along with the derivative. (Inset) Siliceous Beta and H-Beta Si/Al = 19 unit cells are shown alongside each TGA trace. Yellow region represents the sublimation temperature range for pure 5FU.
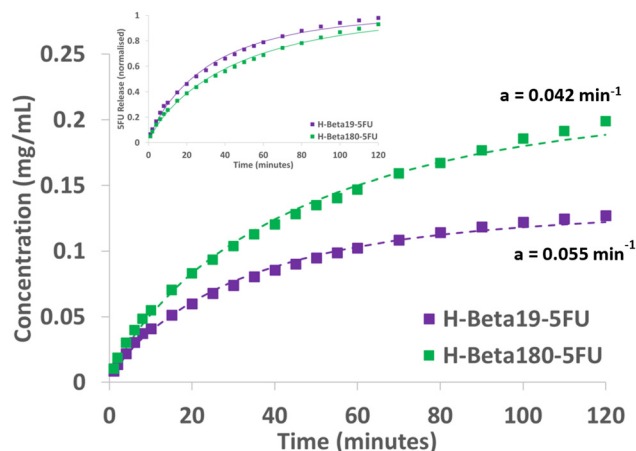
Fig. 3 Release profiles of H-Beta19-5FU (purple) and H-Beta180-5FU (green) obtained in PBS at pH 7.4 at room temperature for 120 minutes, with Weibull model fittings (dashed lines). Normalised drug release profiles from which quantitative values for 'a' and 'b' pertaining to the Weibull model were derived (inset). Data were collected in triplicate and averaged.

Several mathematical kinetic models are in use to describe *in vitro* drug dissolution and drug release patterns, readers are directed towards a review by Costa for more information on each model, and other models that were attempted to fit the data are shown in section S3.1, Fig. S7 (ESI†).[60] The Weibull model, shown in eqn (3.1), is employed in this study and is useful for comparing the drug release of matrix-type drug delivery.[61] This model has been used to fit zeolite-based drug delivery systems before, and note that our R^2 values of 0.995 for each fit in our study are consistent with studies of controlled drug release from zeolites reported previously.[1,62]

$$\frac{M_t}{M_\infty} = 1 - \exp\left(-at^b\right) \tag{3.1}$$

In the Weibull model of drug release, two parameters are calculated: the a parameter refers to the scale and therefore the time dependence of the release, and b which refers to the shape of the curve and is an indicator of the mechanism of transport. A b value of <1 indicates a decelerating release rate, with a higher initial slope ('burst') with the release rate slowing over time thereafter. The a parameter for the H-Beta19-5FU system was 0.055 min^{-1} and that for the H-Beta180-5FU system was 0.042 min^{-1}, denoting a $\sim$30% higher time-dependent release term in the zeolite system with a lower Si/Al ratio, and therefore a slightly faster 'initial burst' from the zeolite with more Brønsted acid sites. These parameters are illustrated more clearly by the plot of drug release normalised to total load (Fig. 3, inset), showing the increased initial release rate from H-Beta19-5FU. The scale parameters are within the range of 5-FU release documented for ZSM-5,[23] where reported time-dependant release parameters were between 0.037 and 0.065 min^{-1} after unit conversion, the former of which was for the protonated form of ZSM-5, which is thus most relevant for comparison rather than those containing sodium counterions. This suggests that release from Beta appears to be faster than from ZSM-5, perhaps due to a greater barrier to diffusion in the smaller pore system of ZSM-5.

The b parameter for the H-Beta19-5FU system was 0.48, and that for the H-Beta180-5FU system was 0.55. Both b values are <1, so the drug release in both samples decelerated over time (common in diffusion-controlled release systems). Since the b parameter for H-Beta180-5FU was slightly closer to 1, this sample had a slightly steadier release profile after the initial burst compared to H-Beta19-5FU, which decelerated more quickly. The relatively faster initial release from H-Beta-19 (followed by a more significant deceleration) could well be due to the drug diffusing in a less hindered fashion through the pore network. While an increase in mobility may be inconsistent with the far higher concentration of strongly adsorbing Brønsted acid sites in the H-Beta-19 pore system compared to H-Beta-180, it could well be consistent with the decreased loading level in this sample observed by TGA, which would lead to less steric hindrance (or molecular 'crowding') from 5FU–5FU interactions, enabling increased mobility through the
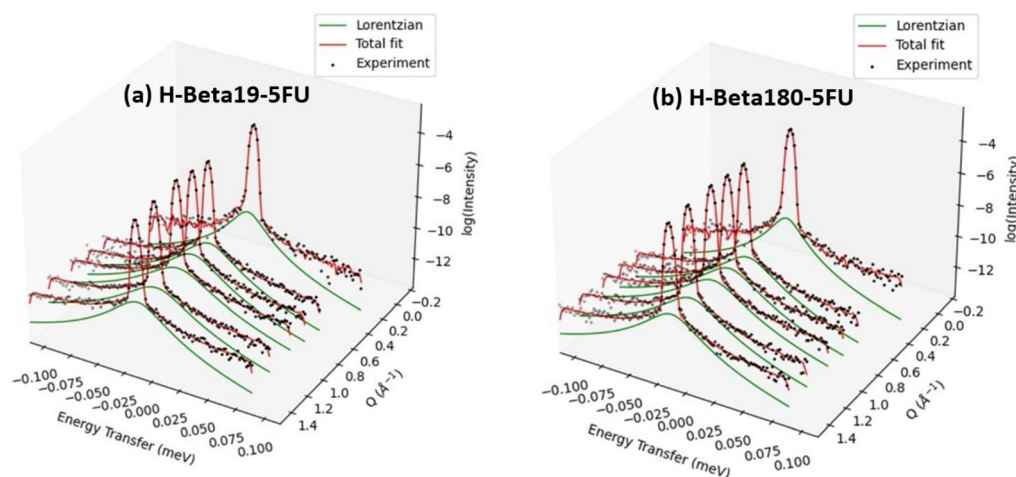

Fig. 4 (a) Subtracted log intensity QENS spectra of (a) H-Beta19-5FU, and (b) H-Beta180-5FU DDSs.

This journal is © The Royal Society of Chemistry 2025

J. Mater. Chem. B, 2025, 13, 10314–10330 | 10319

pore system and out of the material. The relationship between drug release profile and the dynamics/mobility of the drug molecules in the zeolite pores will now be further investigated.

3.3 QENS experiments

QENS spectra of 5FU in the H-Beta19-5FU and H-Beta180-5FU DDSs (with the signal from the empty frameworks subtracted) are shown in Fig. 4a and b respectively. The scattering functions were fit to a delta function convoluted with the resolution measurement at 2 K (which comprises the resolution function accounting for elastic scattering and therefore protons which are 'static' over the timescale probed by the instrument), a single Lorentzian function (convoluted with the resolution measurement) to fit the quasielastic broadening, and a flat background to account for motions too fast to be captured within the instrumental window and the Debye-Waller factor.

Large elastic peaks were observed at all Q values, suggesting that a large proportion of the drug molecules are immobile on the timescale of the instrument, or that localised motions may be taking place.

3.3.1 Modes of motion: EISF analysis. Localised motions may be probed by calculating and fitting the elastic incoherent structure factor (EISF) which is given by:

$$A_0(Q) = \frac{I_{elastic}(Q)}{I_{elastic}(Q) + I_{inelastic}(Q)} \quad (3.2)$$

The EISF is the proportion of total scattered intensity which is elastic and gives information about the type and geometry of localised motion taking place in the DDS. A number of models may be fit to the experimental EISF, which characterise different sorbate behaviours in the zeolite host. These models are shown in Fig. 5 and include isotropic rotation (random full molecule rotation about the centre of mass),[63] the uniaxial rotation of 5FU around a single axis,[64,65] or diffusion confined to a sphere of a specific radius as modelled by the Volino–Dianoux model[66] which details a molecule translating (in the case of a zeolite) in a confining cage.[67,68] Further information about the different models can be found in other resources.[69]

The experimental EISFs (and the best fits of the aforementioned models) of 5FU in H-Beta-19 and H-Beta-180 at 300 K are shown in Fig. 6a and b respectively. The pure models (without consideration for an immobile fraction) for each EISF are fit
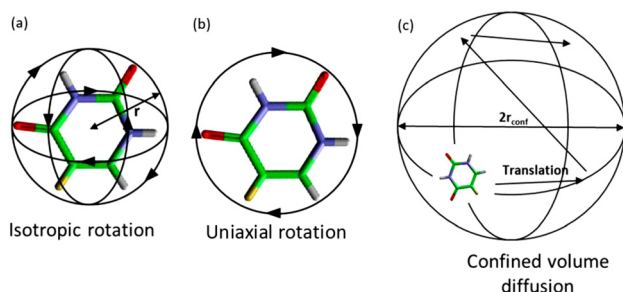

Fig. 5 (a) Isotropic rotation of a 5FU molecule with a radius of rotation r. (b) Uniaxial rotation of the 5FU molecule. (c) Translational motion of protons confined to a spherical volume of radius, r_{conf}.
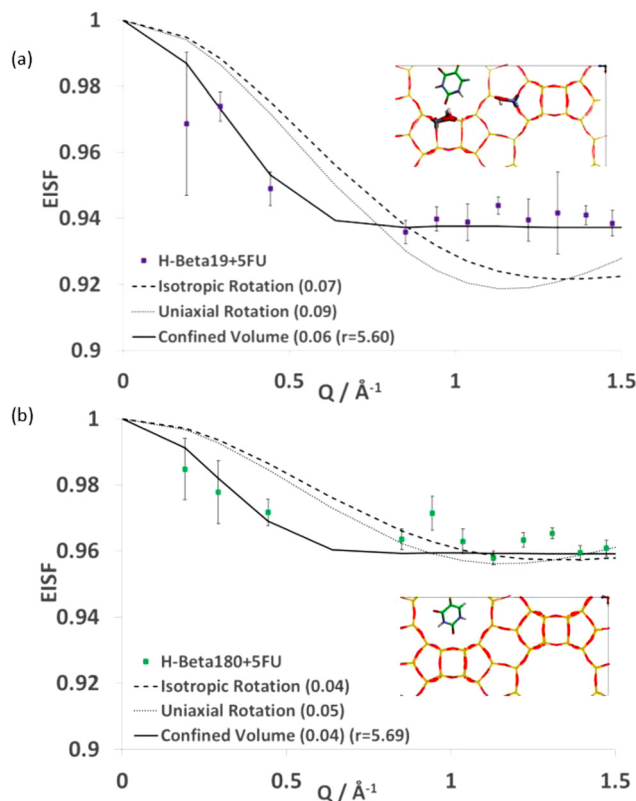

Fig. 6 Experimental EISF plot for 5FU in the (a) H-Beta19-5FU DDS and (b) H-Beta180-5FU DDS at 300 K, including models (mobile fractions shown in the legend in brackets).

against the data in Fig. S8 (ESI†). They do not give acceptable fits to the experimental EISF, and all fall well below the experimental data points at all Q values. The scattering of the experimental data are more elastic than each pure EISF model accounts for, indicating that any motion is heavily constrained in the zeolite structure. This can be accounted for by the incorporation of an immobile fraction of molecules into the EISF fitting, which scales the EISF ($A_0(Q)$) to account for a proportion of immobile molecules resulting in an effective EISF ($A_0^{eff}(Q)$). Given by eqn (3.3).

$$A_0^{eff}(Q) = p_x[A_0(Q)] + (1 - p_x) \quad (3.3)$$

Here, p_x is the fraction of mobile molecules. When an immobile fraction is incorporated into the calculation of the EISF, the model of best fit for H-Beta19-5FU DDS is the Volino–Dianoux model of diffusion confined to a sphere, with the sphere radius of ~ 5.6 Å, Fig. 6. This radius is commensurate to that of the intersection between channels present in zeolite Beta. A best fitting mobile fraction of 6% indicates that the vast majority of the drug molecules are immobile on the timescale of the instrument (~ 300 ps), and the free molecules are diffusing in the channel intersections. Note that some data points were lost due to the subtraction of Bragg peaks which are more significant in the empty zeolite sample, leading to negative intensity in the subtracted QENS spectrum, however, from the possible models of motion for such a system, only the

10320 | J. Mater. Chem. B, 2025, **13**, 10314–10330

This journal is © The Royal Society of Chemistry 2025

Volino–Dianoux model provides an acceptable fit to the data. For isotropic and uniaxial rotation, an acceptable fit was not achieved when allowing the radius of rotation to vary, nor when it was fixed to the molecular radius of 5FU ($\sim$2.4 Å), shown in Fig. 6. Moreover, EISF decay at low Q values is indicative of translational diffusion occurring over distances which are longer than those associated with molecular rotation.

The behaviour of 5FU within the H-Beta180-5FU DDS is now considered. After fitting the EISF to all the models as described for H-Beta19-5FU, the best fitting model is also that of diffusion confined to a sphere with a radius of 5.6 Å. Again, it was necessary to incorporate a mobile fraction into the fitting of the EISF as shown in Fig. S8 (ESI†). The mobile fraction found to best fit the experimental points was 4%, which is lower than that found in the H-Beta19-5FU DDS. The lower mobile population of molecules in the H-Beta180-5FU system is consistent with the slightly slower release rate observed in this sample, and further supports our suggestion that the significantly higher molecular loading level of 5FU in the H-Beta180-5FU system is the significant factor in hindering diffusion, rather than the concentration of strongly adsorbing Brønsted acid sites (which is higher in H-Beta-19 system). Steric hindrance caused by molecule–molecule interactions in the pore system are well known to slow the diffusivity of confined molecules in these systems after a critical point,[70–72] including in nanoporous drug delivery systems,[18] and may lead to a lower number of molecules which are visibly mobile over the timescale of the instrument. It should be noted that other nanoporous systems have completely different pore structures and thus loaded molecules do not necessarily show the same properties. However, this effect of loading level on diffusivity is well documented in the literature, even for smaller molecules. Examples include for water in zeolite MFI,[70] which was shown to have D_s values higher by a factor of $\sim$1.5 in lower loaded systems than when approaching saturation, and for methanol in Beta, where the D_s decreased by a factor of 1.5–2 when the loading was doubled.[72] This effect is also observed for larger molecules such as benzene in zeolite Beta, where increasing the loading from 1 benzene per unit cell to 3 decreased the relative D_s by $\sim$30%.[71] Specific to drug delivery, the effect of drug loading level on the diffusion of encapsulated drug molecules inside porous delivery systems is not well documented. However, one study found that increasing drug loading of diltiazem inside a swellable layered delivery system did not have any impact on drug release.[73] Conversely, another study found that at excessively high drug concentrations, drug molecules block the pores of mesoporous silica (MPS), impacting the diffusion of the drug into the pores and thus the loading level.[74] The effect of drug loading on drug dynamical behaviour and release therefore appears to be very complex and differs from one DDS material to another.

3.3.2 Rates of motion: HWHM analysis. To determine the rate of localised motion, the half-width at half-maximum (HWHM) of the quasielastic Lorentzian fit component as a function of Q^2 is analysed[30] and plotted for H-Beta19-5FU DDS at 300 K in Fig. 7a. The broadenings corroborate the model of

jump diffusion confined to a sphere. For groups fit above $Q^2 = 0.3$ Å^{-2}, the broadenings of the Lorentzian component fit the Singwi–Sjolander jump model,[75] with a jump distance of 2 Å and a residence time of 28 ps. There is a plateauing of the broadenings for the data points at and below $Q^2 = 0.3$ Å^{-2}. According to the Volino–Dianoux model of diffusion confined to a sphere, the plateauing takes place at a Q value corresponding to the diameter of the sphere of confinement ($Q = \pi/r_{conf}$),[66] which in this case is between $Q = 0.44$–0.83 Å^{-1} which may correspond to a sphere with a radius in between 3.8 and 7.1 Å. The intersections of the channels of zeolite Beta are $\sim$11 Å in diameter; therefore, the radius falls within this window, validating the optimal fitting of the EISF to a spherical radius of 5.6 Å. The Volino–Dianoux model may be used to calculate a diffusion coefficient (D_s), for a confined system using HWHM $= 4.33\dfrac{D_s}{r_{conf}{}^2}$ at the low Q plateau point, and use $r_{conf} = 5.6$ Å, to obtain the confined self-diffusion coefficient (D_s) value of $\sim$1.6 ($\pm$0.2) $\times$ 10^{-9} m^2 s^{-1}. It is important to note that this confined D_s is a rate of localised motion within the Beta intersections, so should be treated with caution in terms
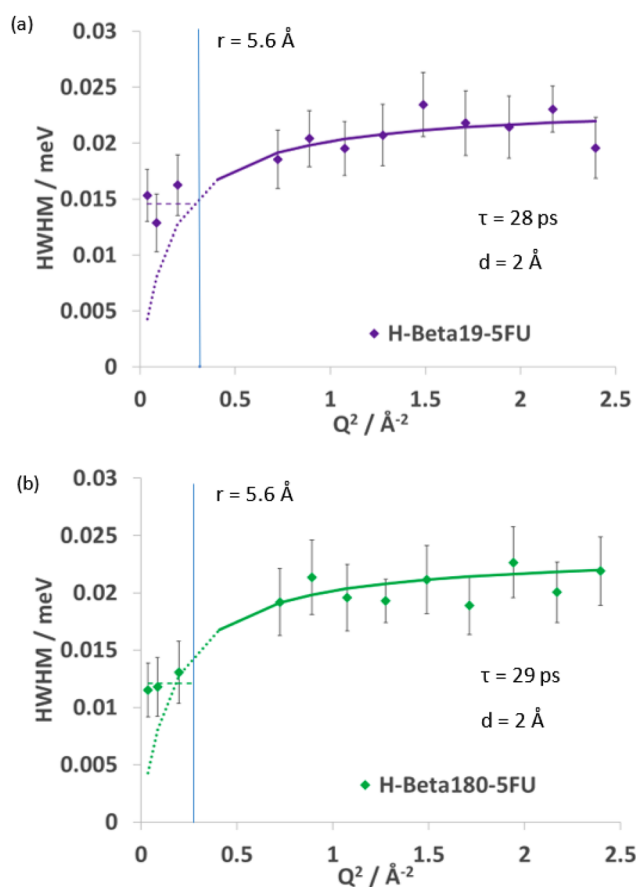

Fig. 7 The Q dependencies of the HWHM of the quasielastic components of the QENS spectra at 300 K for (a) the H-Beta19-5FU DDS and (b) H-Beta180-5FU DDS, their fitting with the Singwi–Sjolander jump model and fitting of low Q values to the Volino–Dianoux confined diffusion model. The Q^2 value corresponding to the radius of the confining sphere is indicated by the blue line.

This journal is © The Royal Society of Chemistry 2025

J. Mater. Chem. B, 2025, **13**, 10314–10330 | **10321**

of drawing comparisons with more conventional diffusion coefficients which measure the long-range diffusion of adsorbates through the zeolite frameworks.

Upon studying the broadenings for the H-Beta180-5FU system (Fig. 7b) the Singwi–Sjolander jump model also best fit the experimental data, with an average jump distance of 2 Å, a residence time of 29 ps and a plateau of broadenings at $Q^2 \leq 0.3$ Å^{-2}, suggesting the same spherical confinement and type of motion as the H-Beta19-5FU system, with a radius of confinement between 3.8–7.1 Å. The jump distance matches that in the H-Beta19-5FU DDS and the residence time is very similar. This suggests that, while the mobile fraction of 5FU molecules is lower in the H-Beta180-5FU system, the molecules which are mobile on the timescale of the instrument are moving at similar rates using the same mechanism in both systems. The diffusion coefficient obtained for this system was 1.3 ($\pm$ 0.3) $\times$ 10^{-9} m^2 s^{-1}, slightly lower than (but within error of) the diffusion coefficient obtained for the H-Beta-19 system. It can therefore be concluded from the line broadenings that, despite a difference in the proportion of mobile molecules over the $\sim$300 ps timescale probed by our spectrometer, the molecules which can move typically diffuse at very similar rates, but slightly slower in the H-Beta180 system. This may be consistent with the lower proportion of molecules able to move in that system as determined by fitting of the EISF, and the slightly lower release rate observed in the controlled release studies.

To summarise, jump diffusion of 5FU confined to the intersections of the H-Beta channels is observed in both systems using our QENS experiments. However, a lower fraction of mobile molecules is observed in the H-Beta180-5FU system despite there being fewer adsorption sites present in this zeolite. The jump diffusion lengths and residence times of 5FU are very similar between both zeolite systems, but the rate of confined diffusion is slightly lower in the H-Beta-180 system. The lower proportion of mobile molecules and slightly lower rates of jump diffusion in the H-Beta-180 system is potentially due to more drug molecules residing in the pores of the zeolite (as observed by both the TGA and controlled release experiments) leading to increased steric hindrance and drug–drug interactions hindering molecular mobility. The observations suggest that the density of adsorption sites is not the primary significant factor in molecular mobility in these structures; rather, the loading level of adsorbate molecules – consistent with the release rates. The effect of loading will be further probed using molecular dynamics simulations in the next section.

3.4 Molecular dynamics simulation analysis

3.4.1 Modes of motion: QENS observables.
Molecular dynamics simulations were analysed focusing on the direct comparison of the localised motions between the simulation and QENS experiments. Note that long-range translational diffusion was not observed in these systems as the mean squared displacement-time plots of 5FU in each system were not linear, in notable contrast to our previous MD studies of

phenol and catechol in the same zeolite framework which showed relatively free diffusion.[76,77]

The self-diffusion coefficients of other aromatics were found to increase significantly (by a factor of 3–10, depending on loadings and temperature) when moving from a siliceous Beta model to those containing increasing concentrations of acid sites, due to the prevalence of adsorbate-acid site H-bonding. A similar relationship may be expected for 5FU in siliceous vs acidic Beta; however, our findings suggest this is not the case, perhaps due to the rigidity of the 5FU molecule, larger size, and the additional polar functional groups present.

To enable direct comparison with QENS experiments, the intermediate scattering function (ISF) was calculated using eqn (2.2) analysing the motions of 5FU within the zeolite pores on the timescale of the QENS instrument. The ISFs were fit to the exponential functions in eqn (2.3). The ISFs calculated from the MD simulation trajectories are shown in Fig. S9 (ESI†) at 300 K for all systems and loadings.

The ''baseline'' of the ISF signifies the value that the decay of the exponential fit to the data approaches where $t = \infty$, and thus it represents the final atomic arrangement in Q space and can be considered as equivalent to the EISF obtained in the QENS experiments. The EISF taken from these baselines can be plotted as a function of Q and fit to the models as described in Section 3.3.1.

Fig. 8 shows the calculated EISF of 5FU in the Beta framework at a loading of 6 wt% at 300 K. Included in Fig. 8 are all the models attempted fit the data. Just as with the QENS experiments, a Volino–Dianoux model of confined diffusion within a sphere gave the best fit to the data across all the investigated systems, indicating that the motion observed is the same between experiment and simulation. The models for isotropic rotation and uniaxial rotation did not produce a satisfactory fit.

When sampling the simulation on the timescale of the QENS spectrometer ($\sim$300 ps), we note that as with experiment, an immobile fraction of molecules is necessary to include into the model fit to the data. The mobile fractions of molecules in the MD calculated EISFs are larger than those observed for the
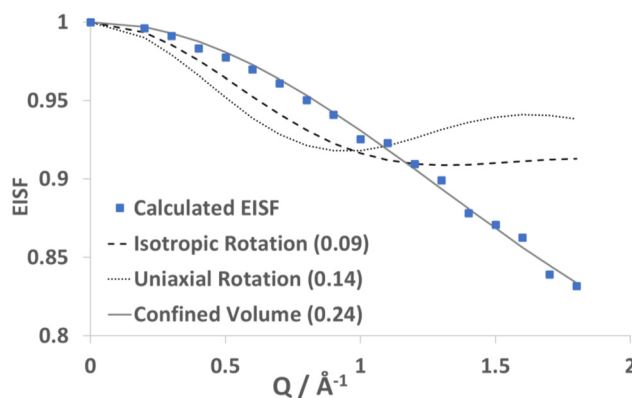

Fig. 8 EISF factor plot obtained from MD simulations for 5FU in the siliceous Beta framework with a loading of 6 wt% at 300 K, with models of motion fit to the calculated values. Mobile fraction values in brackets.

10322 | *J. Mater. Chem. B*, 2025, **13**, 10314–10330

This journal is © The Royal Society of Chemistry 2025

QENS experiment by a factor of *ca.* 3–7, while the confined radius for each system is much lower than the 5.6 Å derived from the QENS experiments (discussed later). We note that the use of CVFF forcefield potentials, which are combined using the Lorentz–Berthelot mixing rules to describe the drug–zeolite interactions, are not widely tested on, or parameterised for this particular system, which could be partially responsible for the quantitative differences between the experimental and simulated results. It is notable that the same form of confined diffusion is observed when the simulations are sampled over the same timescale as the IN16B QENS instrument.

Calculated EISFs of 5FU in the Beta framework with loadings of 6, 10 and 15 wt% are shown in Fig. 9. A clear trend is revealed between loading and molecular mobility of 5FU in the Beta framework. The radius of confinement remains unchanged between the Beta 6 wt% and 10 wt% systems (1.2 Å). Beyond this loading, the radius decreases to 0.9 Å at 15% loading. The low radii of confinement suggest that 5FU moves *via* oscillations or 'rattling' in the Beta pore system, and at the highest loading the radius to which each drug molecule is confined shrinks, due to closer packing. Note that according to the calculated radii in these fittings and their relationship with Q, $\left(Q = \dfrac{\pi}{r_{\mathrm{conf}}}\right)$, the Volino–Dianoux model shape should only begin to appear above Q values of ~ 3 Å^{-1}. EISFs were calculated for each system with Q values up to 10 Å^{-1}, and the fit to the model was maintained above 3 Å^{-1}. Fits up to 2 Å^{-1} are shown for clarity and for comparison with the range sampled by the QENS spectrometer.

From the modelled EISFs it can be concluded that molecular loading level in the pore system has a significant effect on the mobility of encapsulated 5FU and may be predominantly responsible for the difference in mobile fractions observed in our QENS experiments.

Trajectory plots were generated from the production runs, tracking the trajectories of the C–H protons every 1 ps of the

simulation over the course of the 2 ns simulation. Fig. 10 shows an example for Beta at 6 wt% loading, and highlights the tendency for 5FU molecules to congregate in the pore intersections of Beta, where Fig. 10(a) shows a sample configuration taken from the end of the simulation, showing how 5FU molecules had diffused to the intersections, from the individual channels they were initially placed in, over the production run. Fig. 10(b) shows the trajectory plots of 5FU hydrogen atoms throughout the 2 ns production run (post equilibration), showing they are typically located within the channel intersection. These observations complement the QENS results which concluded that 5FU was translating in a confining volume matching that of the Beta intersections. Fig. 10(c) illustrates the area over which hydrogen atoms (green) and the centre of mass (grey) of two representative 5FU molecules oscillate throughout the simulation of Beta with a 6 wt% drug loading. Initial analysis of the oscillation of the 5FU centre of mass implied that the simulations did not agree with the QENS observations, as the radius of confinement was *ca.* 0.5 Å (1.0 Å diameter). However, when probing hydrogen atomic trajectories (which QENS detects directly), strong agreement is observed with the EISF fitting to the Volino–Dianoux model, with a confining radius of 1.2 Å (2.4 Å diameter). In conclusion, 5FU molecules are generally relatively static, exhibiting confined oscillatory motions, where the protons oscillate over a radius of 1.2 Å due to a combination of hindered translational diffusion and rotation.
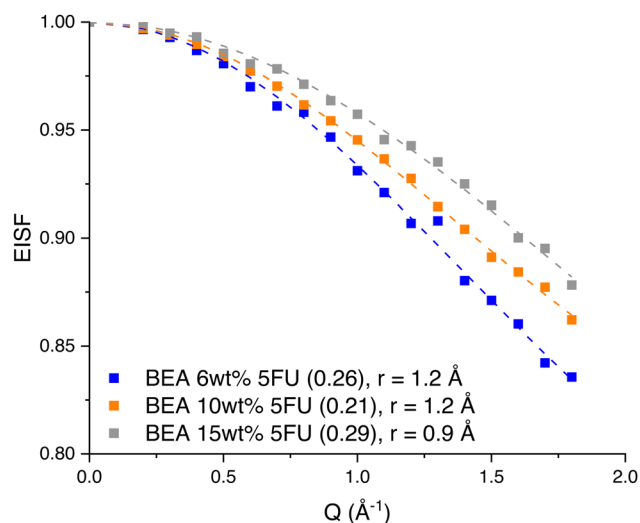

Fig. 9 Combined EISF plots obtained from MD simulations for 5FU in the zeolite Beta framework at 6, 10 and 15 wt% loadings, at 300 K. Mobile fractions in brackets, r = radius of confinement.
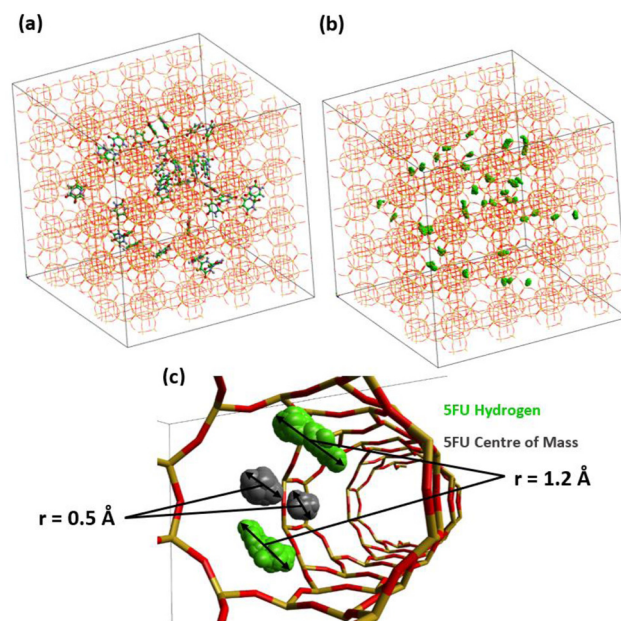

Fig. 10 (a) The final atomic configuration after the 2 ns production run for zeolite Beta at 6 wt% 5FU loading. Positions containing empty space at this visual angle are intersections of the perpendicular channels of Beta, (b) trajectory plot of 5FU hydrogen atoms (coloured green) in the Beta framework with 6 wt% 5FU loading, (c) zoomed-in figure of trajectory plot seen in (b) with additional centre of mass trajectories, demonstrating the diameter of confined diffusion for 2 5FU molecules.

This journal is © The Royal Society of Chemistry 2025

J. Mater. Chem. B, 2025, **13**, 10314–10330 | **10323**

3.4.2 Rates of motion: angular correlation function. A good descriptor for the freedom and rate of a localised motion is the angular correlation function (ACF) which allows us to quantify an approximate rotational diffusion coefficient. The simulation-generated ACFs of 5FU in zeolite Beta with 5FU loadings of 6, 10 and 15 wt% are shown in Fig. 11, along with exponential curve fittings. These are the averaged angular correlation functions of the three 5FU axes in each loaded Beta system over 200 ps. ACFs and fittings for all systems are included in the ESI† (Fig. S10); however, only 6, 10 and 15 wt% are shown below for visual clarity.

For each system, plateaus in the ACFs were reached by ~1 ps; beyond this, small random oscillations were observed. The resulting rotational diffusion coefficients (Table 1) are obtained from the decay constant of the exponential fitting, illustrating the trend in rotational mobility as loading increases. The obtained values are of the same order of magnitude but are lower than the rotational diffusion coefficients derived for similarly sized organic molecules inside zeolite Beta in the literature, such as *para* and *meta*-cresol (6.23–8.46 × 10^{10} s^{-1}),[32] possibly due to the increased mass of the 5FU molecule, loading differences, or increased interactions with the zeolite pore walls due to the increased number of polar functional groups allowing for stronger interactions.

The trend in rotational diffusion coefficients is in agreement with the trend in mobile populations calculated from the EISFs, in that an increase in molecular loading level leads to a decrease in molecular mobility in terms of both the population of mobile molecules and the rates of rotation observed, where increases in loading result in further restriction of rotational mobility of 5FU. The 5FU–5FU interactions which could lead to this restriction are further investigated using RDF analysis in the next section.

3.4.3 Molecular interactions. To probe the interactions between the drug molecule and the zeolite framework, and the interactions between drug molecules themselves in the pore

Table 1 Rotational diffusion coefficients for 5FU in siliceous Beta (4, 6, 10 and 15 wt% loadings) at 300 K

DDS	$D_{rot}/10^{10}$ s^{-1}
Beta 4 wt%	1.93
Beta 6 wt%	1.64
Beta 10 wt%	1.64
Beta 15 wt%	1.54

system throughout the MD simulations, radial distribution functions (RDFs) were generated between relevant atoms.

Fig. 12 is the normalised RDF between zeolite Beta framework oxygen atoms and the amide H atoms on 5FU (which are likely to form hydrogen bonds) at 6, 10 and 15 wt% drug loading. We note that the peaks are typically very well defined for the lower (6 wt%) drug loading but this definition is smoothed at higher loadings, suggesting that 5FU molecules interact with the pore walls with a higher degree of structural order at lower loadings, whereas at higher loadings this structure is less defined, possibly due to increased prevalence of dynamic 5FU–5FU interactions in the system with higher molecular loading. Peaks for the 6 wt% loaded system are exhibited at relatively higher $G(r)$ values at the lowest distances, for example the first notable peak is at 2.3 Å in the 6 wt% system, but at 3.2 Å and 3.7 Å at higher loadings. This indicates that the strongest hydrogen bond remains uninterrupted at lower loadings, but is disturbed at higher loadings which, again, could be due to the presence of additional drug–drug interactions interrupting the most favourable hydrogen bonds. Indeed, the 5FU may have a preference to interact with other 5FU molecules over the pore wall, since it has the tendency to form energetically favourable hydrogen bonded dimers.[78]

Recent DFT calculations probing 5FU adsorption to Brønsted acid sites in FAU zeolites indicate that very strong hydrogen bonding occurs between 5FU and acid sites,[22] with adsorption bond lengths between the 5FU carbonyl groups and
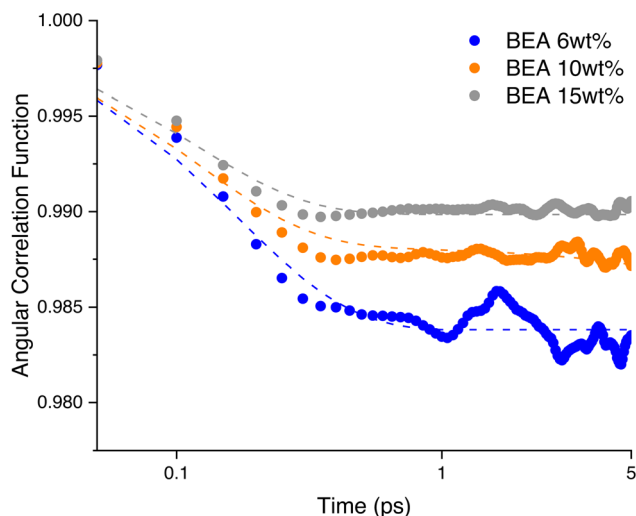

Fig. 11 Combined logarithmic angular correlation function plots obtained from MD simulations for 5FU rotating in siliceous Beta at 6, 10 and 15 wt% loadings, 300 K.
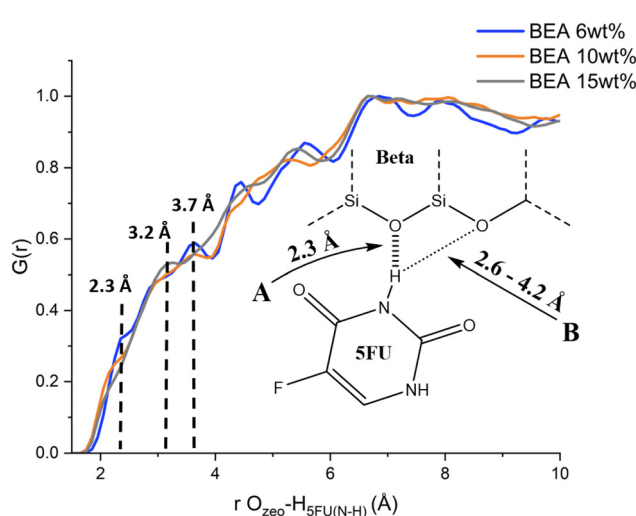

Fig. 12 RDF between framework oxygen and 5FU amide hydrogens (N–H), in zeolite Beta, with 6, 10 and 15 wt% drug loadings with inset diagram depicting the interaction probed.

10324 | *J. Mater. Chem. B*, 2025, **13**, 10314–10330

This journal is © The Royal Society of Chemistry 2025

the acid site itself ranging 1.37–1.55 Å in length. This indicates that the presence of acid sites results in significant additional hydrogen bonding and electrostatic interactions, resulting in stronger 5FU adsorption in the zeolite pores. This is corroborated by the difference in computed adsorption energies: -73 kJ mol^{-1} in siliceous FAU and -144 kJ mol^{-1} when an acid site is present, indicating strong adsorption. Recent adsorption energetics studies on similar sized molecules suggest that these H-bonding interactions would be even stronger in H-Beta compared to H-FAU due to the smaller pore size.[79]

5FU–5FU interactions were probed by generating RDFs between the six-membered rings of 5FU. Fig. 13 is an averaged RDF between the atoms of the six-membered ring in 5-FU, generated for drug loadings of 6, 10 and 15 wt%. A significant interaction is observed at *ca.* 3.4 Å for 5FU in Beta with a 6% loading, labelled in Fig. 13. This initial peak indicates that 5FU molecules interact strongly with each other, most likely by a π-stacking mechanism between the aromatic rings (as shown in Fig. 13 inset), coupled with H-bonding between 5FU oxygen and hydrogen atoms in some orientations. A similar initial peak is observed for the systems with loadings of 10 and 15 wt%, although the distance it occurs at is around 3.7 Å (in line with a peak shoulder occurring at 3.4 Å in the 6 wt% system). This could well be related to a more general increase in steric hindrance with loading, given that in the 6 wt% system face-to-face dimers (see Fig. 13) are able to fit optimally in the Beta intersections uninterrupted. However, as loading is increased towards 5 molecules per unit cell, this optimal interacting configuration is interrupted to maximise the number of 5FU–5FU interactions, as illustrated by the highlighted green region in Fig. 13. Here, a second coordination sphere for the 5FU–5FU interactions emerges, which is not observed at the lower

loading, suggesting that each drug molecule has a tendency to interact with multiple 5FU molecules simultaneously, rather than solely forming one strong interaction between two 5FU molecules. Additionally, the relative height (or proportion of total RDF integration) and sharp definition of the initial 3.4 Å peak in the system with a 6 wt% loading implies that fewer molecules deviate from this specific interaction type in this system, whereas at higher loadings, more interactions fall into the green coordination sphere at *ca.* 4.5–5.5 Å. It is worth noting that the 'face-to-face' dimer coordinations observed in our simulations are not the conventional 5FU dimer, which refers to a side-by-side double hydrogen bonding interaction which does not form due to spatial constraints by the pores.[78]

The dependence of confined translational diffusion and rotational mobility on loading from our QENS experiments can therefore be explained by the prevalence of 5FU–5FU interactions. As loading increases, movement of drug molecules is restricted in the pore system as they maximise the number of favourable 5FU–5FU interactions. The observations that the increases in 5FU–5FU interactions (which are a consequence of the higher molecular loading) slow the local molecular mobility of 5FU in the Beta pore system support the QENS observations that fewer molecules are undergoing confined jump diffusion on the timescale of the instrument. The QENS and MD methods therefore support and explain our conclusion that the slightly faster release rate from H-Beta-19 is due to the lower amount encapsulated, thus allowing increased diffusivity out of the pores of this zeolite compared to H-Beta-180.

The 5FU adsorption energy was calculated using zero Kelvin energy minimisation calculations (using the same DLPOLY4 code as for our MD simulations) for 5FU inside a Beta unit cell. The lowest energy adsorbed structure is shown (Fig. S11, ESI†) and briefly detailed in Section S7.1 giving an adsorption energy of -259.8 kJ mol^{-1} (-62.1 kcal mol^{-1}).

The very large adsorption energy derived demonstrates the significant stabilising interactions that emerge from 5FU entering the pores of Beta. 5FU adsorption energies in zeolite faujasite have previously been calculated using DFT (~-150 kJ mol^{-1})[22] indicating that the adsorption interactions measured for 5FU in Beta are relatively strong, corroborating our findings that minimal 5FU diffusion was occurring in zeolite Beta due to strong attractive van der Waals, electrostatic and H-bonding interactions with the framework. The adsorption energy calculated for 5FU in Beta was larger by a factor of ~1.7 than that previously calculated in faujasite using DFT. This may be reflective of the increased number of interactions occurring between 5FU and the Beta framework due to the smaller pore size. However, it is far more likely to be due to the different methodologies employed, where 5FU in Beta was modelled using CVFF force-fields and calculations for 5FU in faujasite were based on QM methods, so any direct comparisons are not valid (and were not the goal of our particular adsorption calculation), and we lend more credence to QM methods.

Comparison of the rates of motion and the interactions present, probed using RDFs, indicates that diffusion plays a more dominant role than desorption for drug release kinetics.
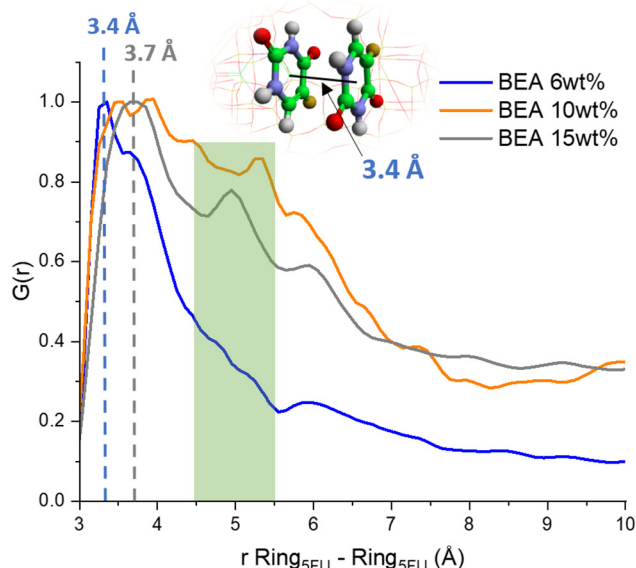

Fig. 13 Averaged RDF between the 6 members of the cyclic component of 5FU, in siliceous Beta at 6, 10 and 15 wt% drug loadings. Simulation snapshot inset to show the interaction described by the RDF and the interaction distance.

This journal is © The Royal Society of Chemistry 2025

J. Mater. Chem. B, 2025, **13**, 10314–10330 | **10325**

We note that in our release measurements, the system with more adsorption sites gave a relatively faster rate of drug release, indicating that another factor is responsible for reducing the release rate in the H-Beta180-5FU system, particularly given the strong adsorption energies calculated by Fischer for 5FU adsorption to acid sites; as large as -183 kJ mol^{-1}.[22] Our subsequent MD analysis indicates that increasing the drug–drug interactions, which increase with drug loading level, significantly impedes 5FU dynamics. The observation is consistent with our drug release measurements where H-Beta180-5FU both released the drug more slowly and had 50% more drug loaded. It is therefore likely to be the secondary effect of loading level and the impediment that the resulting drug–drug interactions impose on diffusion that is slowing 5FU release in this system, rather than a direct effect of desorption from Brønsted acid sites.

Drug diffusion in the Beta pore system appears to be a process of dissolution (in our case, the breaking of drug–drug interactions in the pore system) followed by diffusion, since the Weibull model provided the best fit to the data over various drug release models (a comparison of fittings to different release models is shown in ESI,† Section S3.1, Fig. S7) and our calculated Weibull b parameters of <1 are interpreted as a decreasing or diminishing release rate, typical for diffusion-controlled drug release. Our experimental (QENS) and modelled systems with no water present showed that 5FU was not diffusing a significant amount, thus the effect of solvent may of course be important in determining drug release.

4. Conclusion

The controlled release of anticancer drug 5-fluorouracil (5FU) from two zeolite H-Beta systems, one almost fully siliceous with a Si/Al ratio of 180 (only 0.33 adsorption sites per unit cell) and one with a Si/Al ratio of 19 (with 3 adsorption sites per unit cell), was measured, and correlated with the molecular behaviours and mobility rates of confined 5FU as probed by quasielastic neutron scattering (QENS) and complementary classical molecular dynamics (MD) simulations. Thermogravimetric analysis of the drug delivery systems showed that the more siliceous system (H-Beta180-5FU) had a higher loading capacity by a factor of ~1.5, which was counterintuitive as far fewer adsorption sites are present in this system, and could be attributed to the presence of fewer H-bonded/immobilised 5-FU (or indeed solvent) molecules in the pore system, resulting in a lower hindrance to uptake. The higher drug loading in the H-Beta-180 system had direct consequences in the drug release measurements, with approximately a factor of 1.5 more drug being released from the H-Beta-180 system compared to H-Beta-19 over the measurement time. While the total amount of drug released was higher from the H-Beta-180 system, the relative release rate was faster from the H-Beta-19 system (giving a Weibull model scale parameter of $a = 0.055$ min^{-1} for H-Beta19-5FU compared to 0.042 min^{-1} for H-Beta180-5FU). This observation was again rather counterintuitive given that the H-Beta-19 has a much higher quantity of strongly adsorbing Brønsted acid sites,

but supports the suggestion that the drug could be diffusing in a less hindered fashion through the pore network of H-Beta-19 due to less steric hindrance (or molecular 'crowding') and 5FU–5FU interactions, given the lower loading level of 5FU in H-Beta-19, enabling increased mobility to diffuse out of the zeolite.

Quasielastic neutron scattering experiments investigated the dynamical behaviour of loaded 5FU on the nanoscale. No long-range translational movement on the timescale of the instrument (~300 ps) was observed; however, confined diffusion of the drug within a sphere (with a radius matching that of the intersections between the Beta channels) was observed in both systems, with the EISF fitting to the Volino–Dianoux model of confined diffusion, with a slightly higher mobile fraction in the H-Beta19-5FU system than the H-Beta180-5FU system (with a 6% and 4% fraction of molecules observed respectively). This difference is likely related to the aforementioned higher loading in the H-Beta180-5FU system and resulting steric hindrance to mobility due to molecular 'crowding'. The broadenings of the QENS spectra fit to a confined jump diffusion model supporting the conclusion of confinement to the channel intersections, with similar localised diffusion coefficients extracted for the observably mobile molecules in both systems. Classical MD simulations were used to reproduce QENS observables, such as the intermediate scattering function and the EISF, while angular correlation functions were used to quantify rotational rates. The same Volino–Dianoux model of confined diffusion was the best fitting model to the MD generated EISFs giving similar trends in mobile fraction with loading to those observed experimentally. Increasing the drug loading significantly reduced rotational motion due to increased occurrences of favourable 5FU–5FU interactions in the pore system as probed by RDF analysis, even though the strongest 5FU–zeolite interactions, and the strongest 5FU–5FU H-bonds were disturbed by the presence of a higher quantity of these favourable intermolecular interactions at higher loadings. The increased 5FU–5FU interactions at higher molecular loadings and resulting decreases in mobility, both in the MD simulations and QENS experiments, support the explanation of the faster release rate of 5FU from the H-Beta-19 zeolite being due to increased freedom of mobility in the pore system due to the lower level of molecular loading compared to H-Beta-180, despite the larger concentration of adsorption sites.

The study highlights the complex interplay between zeolite composition, loading level, molecular mobility and resulting release profiles – presenting the critical role of drug–drug interactions in the pore system upon confinement in microporous materials such as zeolites which may be used for controlled release dosage forms.

Conflicts of interest

There are no conflicts to declare.

Data availability

Data for this article, including raw quasielastic neutron scattering data for the experiment 7-05-531, are available at the following DOI: **https://doi.ill.fr/10.5291/ILL-DATA.7-05-531**.

10326 | *J. Mater. Chem. B*, 2025, **13**, 10314–10330

This journal is © The Royal Society of Chemistry 2025

Acknowledgements

References

1 N. Vilaça, R. Amorim, A. F. Machado, P. Parpot, M. F. R. Pereira, M. Sardo, J. Rocha, A. M. Fonseca, I. C. Neves and F. Baltazar, Potentiation of 5-Fluorouracil Encapsulated in Zeolites as Drug Delivery Systems for in Vitro Models of Colorectal Carcinoma, *Colloids Surf., B*, 2013, **112**, 237–244, DOI: 10.1016/J.COLSURFB.2013.07.042.

2 M. Servatan, P. Zarrintaj, G. Mahmodi, S.-J. Kim, M. R. Ganjali, M. R. Saeb and M. Mozafari, Zeolites in Drug Delivery: Progress, Challenges and Opportunities, *Drug Discovery Today*, 2020, **25**(4), 642–656, DOI: 10.1016/j.drudis.2020.02.005.

3 M. Arruebo, Drug Delivery from Structured Porous Inorganic Materials, *Wiley Interdiscip. Rev.:Nanomed. Nanobiotechnol.*, 2012, 16–30, DOI: 10.1002/wnan.132.

4 A. T. Florence and V. H. L. Lee, Commentary Personalised Medicines: More Tailored Drugs, More Tailored Delivery, *Int. J. Pharm.*, 2011, **415**, 29–33, DOI: 10.1016/j.ijpharm.2011.04.047.

5 Strategies to Modify the Drug Release from Pharmaceutical Systems, *Woodhead Publishing series in biomedicine*, ed. M. L. Bruschi, Woodhead Publishing Limited is an imprint of Elsevier, Cambridge, UK, 2015.

6 A. Shahiwala, Formulation Approaches in Enhancement of Patient Compliance to Oral Drug Therapy, *Expert Opin. Drug Delivery*, 2011, **8**(11), 1521–1529, DOI: 10.1517/17425247.2011.628311.

7 5-Fluorouracil | C4H3FN2O2 – PubChem. https://pubchem.ncbi.nlm.nih.gov/compound/5-Fluorouracil (accessed 2020-09-25).

8 E. Sayed, R. Haj-Ahmad, K. Ruparelia, M. S. Arshad, M. W. Chang and Z. Ahmad, Porous Inorganic Drug Delivery Systems—a Review, *AAPS PharmSciTech*, 2017, **18**(5), 1507–1525, DOI: 10.1208/s12249-017-0740-2.

9 H. Alhmoud, B. Delalat, R. Elnathan, A. Cifuentes-Rius, A. Chaix, M.-L. Rogers, J.-O. Durand and N. H. Voelcker, Porous Silicon Nanodiscs for Targeted Drug Delivery, *Adv. Funct. Mater.*, 2015, **25**(7), 1137–1145, DOI: 10.1002/adfm.201403414.

10 C. Bharti, N. Gulati, U. Nagaich and A. Pal, Mesoporous Silica Nanoparticles in Target Drug Delivery System: A Review, *Int. J. Pharm. Invest.*, 2015, **5**(3), 124, DOI: 10.4103/2230-973x.160844.

11 Z. Jiang, Y. Li, Z. Wei, B. Yuan, Y. Wang, O. U. Akakuru, Y. Li, J. Li and A. Wu, Pressure-Induced Amorphous Zeolitic Imidazole Frameworks with Reduced Toxicity and Increased Tumor Accumulation Improves Therapeutic Efficacy In Vivo, *Bioact. Mater.*, 2021, **6**(3), 740–748, DOI: 10.1016/j.bioactmat.2020.08.036.

12 E. H. C. Silva, E. S. M. Cutrim, M. R. C. Iemma, H. S. Barud, A. Rojas, L. Gómez-Hortigüela, A. S. de Menezes, E. Rodríguez-Castellón, A. A. Tanaka and A. C. S. Alcântara, New Insights about the Intercalation of 5-Fluorouracil into 2D Mg–Al Layered Double Hydroxide Nanosheets: A Theoretical and Experimental Investigation, *J. Drug Delivery Sci. Technol.*, 2023, **81**, 104294, DOI: 10.1016/j.jddst.2023.104294.

13 E. S. M. Cutrim, A. A. M. Vale, D. Manzani, H. S. Barud, E. Rodríguez-Castellón, A. P. S. A. Santos and A. C. S. Alcântara, Preparation, Characterization and in Vitro Anticancer Performance of Nanoconjugate Based on Carbon Quantum Dots and 5-Fluorouracil, *Mater. Sci. Eng., C*, 2021, **120**, 111781, DOI: 10.1016/j.msec.2020.111781.

14 M. Khodadadi Yazdi, P. Zarrintaj, H. Hosseiniamoli, A. H. Mashhadzadeh, M. R. Saeb, J. D. Ramsey, M. R. Ganjali and M. Mozafari, Zeolites for Theranostic Applications, *J. Mater. Chem. B*, 2020, **8**(28), 5992–6012, DOI: 10.1039/d0tb00719f.

15 L. Bacakova, M. Vandrovcova, I. Kopova and I. Jirka, Applications of Zeolites in Biotechnology and Medicine – a Review, *Biomater. Sci.*, 2018, **6**(5), 974–989, DOI: 10.1039/C8BM00028J.

16 R. Diab, N. Canilho, I. A. Pavel, F. B. Haffner, M. Girardon and A. Pasc, Silica-Based Systems for Oral Delivery of Drugs, Macromolecules and Cells, *Adv. Colloid Interface Sci.*, 2017, **249**, 346–362, DOI: 10.1016/j.cis.2017.04.005.

17 J. Liu and J. Yu Toward Greener and Designed Synthesis of Zeolite Materials, in *Zeolite and Zeolite-like Materials*, ed. B. F. Sels and L. M. Kustov, Elsevier, 2016, pp. 1–32.

18 A. J. Wise, J. S. Sefy, E. Barbu, A. J. O'Malley, S. M. Van Der Merwe and P. A. Cox, Zero-Order and Prolonged Release of Atenolol from Microporous FAU and BEA Zeolites, and Mesoporous MCM-41: Experimental and Theoretical Investigations, *J. Controlled Release*, 2020, **327**, 140–149, DOI: 10.1016/j.jconrel.2020.07.027.

19 M. Spanakis, N. Bouropoulos, D. Theodoropoulos, L. Sygellou, S. Ewart, A. M. Moschovi, A. Siokou, I. Niopas, K. Kachrimanis, V. Nikolakis, P. A. Cox, I. S. Vizirianakis and D. G. Fatouros, Controlled Release of 5-Fluorouracil

This journal is © The Royal Society of Chemistry 2025

J. Mater. Chem. B, 2025, **13**, 10314–10330 | **10327**

from Microporous Zeolites, *Nanomedicine*, 2014, **10**(1), 197–205, DOI: 10.1016/j.nano.2013.06.016.

20 N. Vilaça, F. Morais-Santos, A. F. Machado, A. Sirkecioğlu, M. F. R. Pereira, M. Sardo, J. Rocha, P. Parpot, A. M. Fonseca, F. Baltazar and I. C. Neves, Micro- and Mesoporous Structures as Drug Delivery Carriers for Salicylic Acid, *J. Phys. Chem. C*, 2015, **119**(7), 3589–3595, DOI: 10.1021/jp5117849.

21 A. Datt, E. A. Burns, N. A. Dhuna and S. C. Larsen, Loading and Release of 5-Fluorouracil from HY Zeolites with Varying SiO2/Al2O3 Ratios, *Microporous Mesoporous Mater.*, 2013, **167**, 182–187, DOI: 10.1016/J.MICROMESO.2012.09.011.

22 M. Fischer, Adsorption of 5-Fluorouracil, an Anticancer Drug, in Faujasite-Type Zeolites: Understanding Storage and Release with Density Functional Theory Calculations, *CrystEngComm*, 2024, **26**(28), 3795–3807, DOI: 10.1039/D4CE00344F.

23 R. A. Al-Thawabeia and H. A. Hodali, Use of Zeolite ZSM-5 for Loading and Release of 5-Fluorouracil, *J. Chem.*, 2015, **2015**, 1–9, DOI: 10.1155/2015/403597.

24 A. J. O'Malley, S. F. Parker and C. R. A. Catlow, Neutron Spectroscopy as a Tool in Catalytic Science, *Chem. Commun.*, 2017, **53**(90), 12164–12176, DOI: 10.1039/c7cc05982e.

25 H. Jobic Diffusion Studies Using Quasi-Elastic Neutron Scattering, *Membrane Science and Technology*, Elsevier, 2000, vol. 6, pp. 109–137, DOI: 10.1016/S0927-5193(00)80007-8.

26 S. Mitra, V. K. Sharma and R. Mukhopadhyay, Diffusion of Confined Fluids in Microporous Zeolites and Clay Materials, *Rep. Prog. Phys.*, 2021, **84**(6), 066501, DOI: 10.1088/1361-6633/abf085.

27 A. J. O'Malley, V. García Sakai, N. Dimitratos, W. Jones, C. R. A. Catlow and S. F. Parker, Octane Isomer Dynamics in H-ZSM-5 as a Function of Si/Al Ratio: A Quasi-Elastic Neutron Scattering Study, *Philos. Trans. R. Soc., A*, 2020, **378**(2176), 20200063, DOI: 10.1098/rsta.2020.0063.

28 R. Mukhopadhyay, A. Sayeed, S. Mitra, A. V. Anil Kumar, M. N. Rao, S. Yashonath and S. L. Chaplot, Rotational Dynamics of Propane in Na-Y Zeolite: A Molecular Dynamics and Quasielastic Neutron-Scattering Study, *Phys. Rev. E:Stat., Nonlinear, Soft Matter Phys.*, 2002, **66**(6), 061201, DOI: 10.1103/PhysRevE.66.061201.

29 R. M. Edkins, M. Appel, T. Seydel and K. Edkins, The Modifying Effect of Supramolecular Gel Fibres on the Diffusion of Paracetamol and Ibuprofen Sodium on the Picosecond Timescale, *Phys. Chem. Chem. Phys.*, 2020, **22**(19), 10838–10844, DOI: 10.1039/D0CP01240H.

30 H. Jobic and D. N. Theodorou, Quasi-Elastic Neutron Scattering and Molecular Dynamics Simulation as Complementary Techniques for Studying Diffusion in Zeolites, *Microporous Mesoporous Mater.*, 2007, **102**(1–3), 21–50, DOI: 10.1016/J.MICROMESO.2006.12.034.

31 A. J. O'Malley and C. Catlow Sorbate Dynamics in Zeolite Catalysts, in *Nuetron Scattering – Applications in Biology, Chemistry, and Materials Science, Experimental Methods in the Physical Sciences*, ed. F. P. D. Fernandez-Alonso, Academic Press, 2017, ch. 6, pp. 349–401.

32 K. S. C. Morton, A. J. Porter, J. Armstrong and A. J. O'Malley, The Effect of Molecular Shape and Pore Structure on Local and Nanoscale Cresol Behaviour in Commercial Zeolite Catalysts, *Catal. Sci. Technol.*, 2024, **14**(13), 3756–3770, DOI: 10.1039/D4CY00321G.

33 H. Jobic, A. N. Fitch and J. Combet, Diffusion of Benzene in NaX and NaY Zeolites Studied by Quasi-Elastic Neutron Scattering, *J. Phys. Chem. B*, 2000, **104**(35), 8491–8497, DOI: 10.1021/jp000994f.

34 A. K. Tripathi, A. Sahasrabudhe, S. Mitra, R. Mukhopadhyay, N. M. Gupta and V. B. Kartha, QENS and FTIR Studies on Binding States of Benzene Molecules Adsorbed in Zeolite HZSM-5 at Room Temperature, *Phys. Chem. Chem. Phys.*, 2001, **3**(19), 4449–4455, DOI: 10.1039/b102055m.

35 K. S. C. Morton, M. Appel, C. L. M. Woodward, J. Armstrong and A. J. O'Malley, The Effect of Pore Structure on the Local and Nanoscale Mobility of Anisole and Guaiacol in Commercial Zeolite Catalysts, *Microporous Mesoporous Mater.*, 2025, **383**, 113388, DOI: 10.1016/j.micromeso.2024.113388.

36 S. Mitra, A. K. Tripathy, N. M. Gupta and R. Mukhopadhyay, Molecular Motions of Benzene Adsorbed in ZSM-5 Zeolite: Quasielastic Neutron Scattering Study, *Appl. Phys. A:Mater. Sci. Process.*, 2002, **74**(0), s1308–s1310, DOI: 10.1007/s003390201378.

37 E. Kontogiannidou, C. Karavasili, M. G. Kouskoura, M. Filippousi, G. Van Tendeloo, I. I. Andreadis, G. K. Eleftheriadis, I. Kontopoulou, C. K. Markopoulou, N. Bouropoulos and D. G. Fatouros, In Vitro and Ex Vivo Assessment of Microporous Faujasite Zeolite (NaX-FAU) as a Carrier for the Oral Delivery of Danazol, *J. Drug Delivery Sci. Technol.*, 2019, **51**, 177–184, DOI: 10.1016/j.jddst.2019.02.036.

38 E. Khodaverdi, H. A. Soleimani, F. Mohammadpour and F. Hadizadeh, Synthetic Zeolites as Controlled-Release Delivery Systems for Anti-Inflammatory Drugs, *Chem. Biol. Drug Des.*, 2016, **87**(6), 849–857, DOI: 10.1111/cbdd.12716.

39 K. A. Fisher, K. D. Huddersman and M. J. Taylor, Comparison of Micro- and Mesoporous Inorganic Materials in the Uptake and Release of the Drug Model Fluorescein and Its Analogues, *Chem. – Eur. J.*, 2003, **9**(23), 5873–5878, DOI: 10.1002/CHEM.200304764.

40 O. Arnold, J. C. Bilheux, J. M. Borreguero, A. Buts, S. I. Campbell, L. Chapon, M. Doucet, N. Draper, R. Ferraz Leal, M. A. Gigg, V. E. Lynch, A. Markvardsen, D. J. Mikkelson, R. L. Mikkelson, R. Miller, K. Palmen, P. Parker, G. Passos, T. G. Perring, P. F. Peterson, S. Ren, M. A. Reuter, A. T. Savici, J. W. Taylor, R. J. Taylor, R. Tolchenov, W. Zhou and J. Zikovsky, Mantid—Data Analysis and Visualization Package for Neutron Scattering and μ SR Experiments, *Nucl. Instrum. Methods Phys. Res., Sect. A*, 2014, **764**, 156–166, DOI: 10.1016/J.NIMA.2014.07.029.

41 R. T. Azuah, L. R. Kneller, Y. Qiu, P. L. W. Tregenna-Piggott, C. M. Brown, J. R. D. Copley and R. M. Dimeo, DAVE: A Comprehensive Software Suite for the Reduction, Visualization, and Analysis of Low Energy Neutron Spectroscopic Data, *J. Res. Natl. Inst. Stand. Technol.*, 2009, **114**(6), 341, DOI: 10.6028/JRES.114.025.

42 W. Hao, W. Zhang, Z. Guo, J. Ma and R. Li, Mesoporous Beta Zeolite Catalysts for Benzylation of Naphthalene: Effect of

10328 | *J. Mater. Chem. B*, 2025, **13**, 10314–10330

This journal is © The Royal Society of Chemistry 2025

Pore Structure and Acidity, *Catalysts*, 2018, **8**(11), 504, DOI: **10.3390/catal8110504**.

43 C. Baerlocher and L. B. McCusker *Database of Zeolite Structures*, **https://www.iza-structure.org/databases/**.

44 J. B. Higgins, R. B. LaPierre, J. L. Schlenker, A. C. Rohrman, J. D. Wood, G. T. Kerr and W. J. Rohrbaugh, The Framework Topology of Zeolite Beta, *Zeolites*, 1988, **8**(6), 446–452, DOI: **10.1016/S0144-2449(88)80219-7**.

45 J. M. Newsam, M. M. J. Treacy, W. T. Koetsier and C. B. De Gruyter, Structural Characterization of Zeolite Beta, *Proc. R. Soc. London, Ser. A*, 1988, **420**(1859), 375–405, DOI: **10.1098/rspa.1988.0131**.

46 A. J. O'Malley and C. R. A. Catlow, Molecular Dynamics Simulations of Longer N-Alkanes in Silicalite: A Comparison of Framework and Hydrocarbon Models, *Phys. Chem. Chem. Phys.*, 2013, **15**(43), 19024, DOI: **10.1039/c3cp52653d**.

47 K. P. Schröder, J. Sauer, M. Leslie, C. Richard, A. Catlow and J. M. Thomas, Bridging Hydrodyl Groups in Zeolitic Catalysts: A Computer Simulation of Their Structure, Vibrational Properties and Acidity in Protonated Faujasites (HY Zeolites), *Chem. Phys. Lett.*, 1992, **188**(3–4), 320–325, DOI: **10.1016/0009-2614(92)90030-Q**.

48 M. J. Sanders; M. Leslie and C. R. A. Catlowb *Interatomic Potentials for SiOa*, 1984.

49 N. A. Ramsahye and R. G. Bell, Cation Mobility and the Sorption of Chloroform in Zeolite NaY: Molecular Dynamics Study, *J. Phys. Chem. B*, 2005, **109**(10), 4738–4747, DOI: **10.1021/jp046958o**.

50 P. Dauber-Osguthorpe, V. A. Roberts, D. J. Osguthorpe, J. Wolff, M. Genest and A. T. Hagler, Structure and Energetics of Ligand Binding to Proteins: Escherichia Coli Dihydrofolate Reductase-Trimethoprim, a Drug-Receptor System, *Proteins: Struct., Funct., Bioinf.*, 1988, **4**(1), 31–47, DOI: **10.1002/PROT.340040106**.

51 Y. Abdel-Mottaleb and M. S. A. Abdel-Mottaleb, Molecular Modeling Studies of Some Uracil and New Deoxyuridine Derivatives, *J. Chem.*, 2016, **2016**, 1–12, DOI: **10.1155/2016/5134732**.

52 E. Generalic Lennard-Jones *potential*. Croatian-English Chemistry Dictionary & Glossary. **https://glossary.periodni.com/glossary.php?en=Lennard-Jones+potential** (accessed 2019-08-22).

53 H. A. Lorentz, Ueber Die Anwendung Des Satzes Vom Virial in Der Kinetischen Theorie Der Gase, *Ann. Phys.*, 1881, **248**(1), 127–136, DOI: **10.1002/andp.18812480110**.

54 I. T. Todorov, W. Smith, K. Trachenko and M. T. Dove, DL_POLY_4 User Manual, *J. Mater. Chem.*, 2006, **16**, 1611–1618.

55 P. P. Ewald, Die Berechnung Optischer Und Elektrostatischer Gitterpotentiale, *Ann. Phys.*, 1921, **369**(3), 253–287, DOI: **10.1002/andp.19213690304**.

56 A. J. Porter, C. H. Botchway, B. Kwakye-Awuah, C. Hernandez-Tamargo, S. K. Matam, S. L. McHugh, I. P. Silverwood, N. H. de Leeuw and A. J. O'Malley, Local and Nanoscale Methanol Mobility in Different H-FER Catalysts, *Catal. Sci. Technol.*, 2022, **12**(5), 1663–1677, DOI: **10.1039/D1CY02001C**.

57 G. Goret, B. Aoun and E. Pellegrini, MDANSE: An Interactive Analysis Environment for Molecular Dynamics Simulations, *J. Chem. Inf. Model.*, 2017, **57**(1), 1–5, DOI: **10.1021/acs.jcim.6b00571**.

58 S. Aliaskarisohi, P. Tierno, P. Dhar, Z. Khattari, M. Blaszczynski and Th. M. Fischer, On the Diffusion of Circular Domains on a Spherical Vesicle, *J. Fluid Mech.*, 2010, **654**, 417–451, DOI: **10.1017/S0022112010000650**.

59 S. Simonetti, A. D. Compañy, E. Pronsato, A. Juan, G. Brizuela and A. Lam, Density Functional Theory Based-Study of 5-Fluorouracil Adsorption on β-Cristobalite (1 1 1) Hydroxylated Surface: The Importance of H-Bonding Interactions, *Appl. Surf. Sci.*, 2015, **359**, 474–479, DOI: **10.1016/j.apsusc.2015.10.147**.

60 P. Costa and J. M. Sousa Lobo, Modeling and Comparison of Dissolution Profiles, *Eur. J. Pharm. Sci.*, 2001, 123–133, DOI: **10.1016/S0928-0987(01)00095-1**.

61 S. Dash, P. N. Murthy, L. Nath and P. Chowdhury, Kinetic Modeling on Drug Release from Controlled Drug Delivery Systems, *Acta Pol. Pharm.*, 2010, **67**(3), 217–223.

62 M. Spanakis, N. Bouropoulos, D. Theodoropoulos, L. Sygellou, S. Ewart, A. M. Moschovi, A. Siokou, I. Niopas, K. Kachrimanis, V. Nikolakis, P. A. Cox, I. S. Vizirianakis and D. G. Fatouros, Controlled Release of 5-Fluorouracil from Microporous Zeolites, *Nanomedicine*, 2014, **10**(1), 197–205, DOI: **10.1016/j.nano.2013.06.016**.

63 V. F. Sears, Theory of cold neutron scattering by homonuclear diatomic liquids: I. Free rotation, *Can. J. Phys.*, 1966, **44**(6), 1279–1297, DOI: **10.1139/P66-108**.

64 H. Jobic, M. Bée and A. J. Dianoux, Quasi-Elastic Neutron Scattering Study of Benzene Adsorbed in ZSM-5, *J. Chem. Soc., Faraday Trans. 1*, 1989, **85**(8), 2525, DOI: **10.1039/f19898502525**.

65 A. J. O'Malley, V. García Sakai, N. Dimitratos, W. Jones, C. R. A. Catlow and S. F. Parker, Octane Isomer Dynamics in H-ZSM-5 as a Function of Si/Al Ratio: A Quasi-Elastic Neutron Scattering Study, *Philos. Trans. R. Soc., A*, 2020, **378**(2176), 20200063, DOI: **10.1098/rsta.2020.0063**.

66 F. Volino and A. J. Dianoux, Neutron Incoherent Scattering Law for Diffusion in a Potential of Spherical Symmetry: General Formalism and Application to Diffusion inside a Sphere, *Mol. Phys.*, 2006, **41**(2), 271–279, DOI: **10.1080/00268978000102761**.

67 A. J. Porter, S. L. McHugh, T. Omojola, I. P. Silverwood and A. J. O'Malley, The Effect of Si/Al Ratio on Local and Nanoscale Water Diffusion in H-ZSM-5: A Quasielastic Neutron Scattering and Molecular Dynamics Simulation Study, *Microporous Mesoporous Mater.*, 2023, **348**, 112391, DOI: **10.1016/j.micromeso.2022.112391**.

68 T. Omojola, I. P. Silverwood and A. J. O'Malley, Molecular Behaviour of Methanol and Dimethyl Ether in H-ZSM-5 Catalysts as a Function of Si/Al Ratio: A Quasielastic Neutron Scattering Study, *Catal. Sci. Technol.*, 2020, **10**(13), 4305–4320, DOI: **10.1039/D0CY00670J**.

69 M. Bée, *Quasielastic Neutron Scattering: Principles and Applications in Solid State Chemistry, Biology and Materials Science*, Adam Hilger, Bristol, Philadelphia, 1988.

70 K. N. Han, S. Bernardi, L. Wang and D. J. Searles, Water Diffusion in Zeolite Membranes: Molecular Dynamics Studies on Effects of Water Loading and Thermostat, *J. Membr. Sci.*, 2015, **495**, 322–333, DOI: **10.1016/j.memsci.2015.08.033**.

71 H. Mohammadi-Manesh, S. Tashakor and S. Alavi, Diffusion of Benzene through the Beta Zeolite Phase, *Microporous Mesoporous Mater.*, 2013, **181**, 29–37, DOI: **10.1016/j.micromeso.2013.07.009**.

72 C. Botchway, R. Tia, E. Adei, A. O'Malley, N. Dzade, C. Hernandez-Tamargo and N. De Leeuw, Influence of Topology and Brønsted Acid Site Presence on Methanol Diffusion in Zeolites Beta and MFI, *Catalysts*, 2020, **10**(11), 1342, DOI: **10.3390/catal10111342**.

73 L. Yang and R. Fassihi, Examination of Drug Solubility, Polymer Types, Hydrodynamics and Loading Dose on Drug Release Behavior from a Triple-Layer Asymmetric Configuration Delivery System, *Int. J. Pharm.*, 1997, **155**(2), 219–229, DOI: **10.1016/S0378-5173(97)00164-6**.

74 A. Budiman, Y. Wardhana, A. Ainurofiq, Y. Nugraha, R. Qaivani, S. Lukmanul Hakim and D. Aulifa, Drug-Coformer Loaded-Mesoporous Silica Nanoparticles: A Review of the Preparation, Characterization, and Mechanism of Drug Release, *Int. J. Nanomed.*, 2024, **19**, 281–305, DOI: **10.2147/IJN.S449159**.

75 K. S. Singwi and A. Sjölander, Diffusive Motions in Water and Cold Neutron Scattering, *Phys. Rev.*, 1960, **119**(3), 863–871, DOI: **10.1103/PhysRev.119.863**.

76 C. Hernandez-Tamargo, A. O'Malley, I. P. Silverwood and N. H. De Leeuw, Molecular Behaviour of Phenol in Zeolite Beta Catalysts as a Function of Acid Site Presence: A Quasielastic Neutron Scattering and Molecular Dynamics Simulation Study, *Catal. Sci. Technol.*, 2019, **9**(23), 6700–6713, DOI: **10.1039/C9CY01548E**.

77 C. Hernandez-Tamargo, I. P. Silverwood, A. J. O'Malley and N. H. D. Leeuw, Quasielastic Neutron Scattering and Molecular Dynamics Simulation Study on the Molecular Behaviour of Catechol in Zeolite Beta, *Top. Catal.*, 2021, **64**(9–12), 707–721, DOI: **10.1007/s11244-020-01400-1**.

78 D. L. Melnikova, Z. F. Badrieva, M. A. Kostin, C. Maller, M. Stas, A. Buczek, M. A. Broda, T. Kupka, A.-M. Kelterer, P. M. Tolstoy and V. D. Skirda, On Complex Formation between 5-Fluorouracil and β-Cyclodextrin in Solution and in the Solid State: IR Markers and Detection of Short-Lived Complexes by Diffusion NMR, *Molecules*, 2020, **25**(23), 5706, DOI: **10.3390/molecules25235706**.

79 K. S. C. Morton, A. J. O. Malley and J. Armstrong, Probing Adsorption Interactions of Lignin Derivatives in Industrial Zeolite Catalysts through Combining Vibrational Spectroscopy and Ab Initio Calculations, *RSC Sustainability*, 2025, **3**(7), 2938–2951, DOI: **10.1039/d5su00024f**.

80 University of Bath. Research Computing. University of Bath 2018, DOI: **10.15125/B6CD-S854**.

10330 | *J. Mater. Chem. B*, 2025, **13**, 10314–10330

This journal is © The Royal Society of Chemistry 2025